Binding of the Nucleocapsid Protein of Type 1 Human Immunodeficiency Virus to Nucleic Acids Studied Using Phosphorescence and Optically Detected Magnetic Resonance†

Jie Q. Wu,‡ Andrzej Ozarowski,‡ August H. Maki,*,‡ Maria A. Urbaneja,§,|| Louis E. Henderson,§ and Jose R. Casas-Finet§

Department of Chemistry, University of California, Davis, California 95616, and AIDS Vaccine Program, SAIC Frederick, National Cancer Institute−Frederick Cancer Research and Development Center, Frederick, Maryland 21702-1201

Received March 24, 1997⊗

ABSTRACT: The binding of p7 nucleocapsid protein of type 1 human immunodeficiency virus (HIV-1) to various oligonucleotides and polynucleotides has been investigated by phosphorescence and optically detected magnetic resonance (ODMR) spectroscopy. The intrinsic spectroscopic probe used in these studies is the photoexcited triplet state of Trp37, which is associated with the C-terminal zinc finger of p7 and is its only tryptophan residue. Complex formation produces a red-shift of the phosphorescence 0,0-band ($\Delta E_{0,0}$) of Trp37 as well as a reduction of the zero field splitting (zfs) D parameter. Increases of $-\Delta E_{0,0}$ (A < C < U < G <I) rank with increasing binding affinity to nucleic acid homooligomers (A ∼ C < U < G ∼ I). It is proposed that the magnitude of the shift reflects the extent of aromatic stacking interactions. We propose also that $-\Delta D$ increases not only with increased aromatic stacking but also with the extent of charge transfer (CT) character admixed into the triplet state. The quantity $\Delta D/\Delta E_{0,0}$ correlates with the electron affinity of the bases (G < A < C < U ≈ T), suggesting that this quantity reflects the extent of CT character admixed with the triplet state by the aromatic stacking interaction. Also affected by nucleic acid binding of p7 are the kinetic parameters of Trp37. We find a selective increase in the relative populating rate, and of the decay rate constant of the T_x sublevel. In binding of p7 to either $d(IT)_2$ or $d(IT)_4$, two distinct sets of triplet states of Trp37 are resolved, suggesting the existence of specific nucleic acid binding modes of these heterooligomers.

Human immunodeficiency virus type 1 (HIV-1)[1] is a member of the lentivirus subfamily of retrovirus. In general, retroviruses utilize RNA as their genomic message and package two plus-strands of genomic RNA into the virion (*1*). After budding from the cell, retroviruses typically undergo morphological rearrangements (maturation) which include a condensation of the genomic RNA into a nucleoprotein complex in the core of the infectious virus. During infection the virus delivers its genomic message to the cell as a nucleoprotein complex (preintegration complex) which includes RNA, reverse transcriptase (RT), integrase (IN), and the viral nucleocapsid (NC) protein. RT transcribes the genomic RNA to double-stranded proviral DNA, and IN catalyzes its integration into the host cell genome (*2*). The NC protein binds to nucleic acids and has numerous roles in the viral replication cycle (*3*). Retroviral NC proteins are synthesized as a domain in polyproteins referred to as Gag precursors. Gag precursors are "self-associating" proteins which function during viral assembly and require the NC domain for specific recognition and packaging of genomic RNA (*4*). In this role, the NC domain exhibits a specific recognition which is probably mediated through binding to specific RNA structures (*5*). During and after budding, the NC protein is cleaved from the precursor by a viral protease (*6*) and condenses with RNA to form the nucleoprotein core of the mature virus. The mature virus contains about 2500 copies of the NC protein bound to 2 RNA strands, each composed of about 9000 nucleotides (or about 7 nucleotides per bound NC protein) (*7*). In this mode, the NC protein exhibits non-sequence-specific binding to single-stranded RNA and promotes the condensation of the RNA into the core structure. During the infectious process, the nucleoprotein complex is taken into the cell where RT transcribes the RNA to double-stranded DNA. Recent mutational analysis revealed the vital role of NC protein in the infectious process (*8*). *In vitro* studies suggest that NC protein facilitates the RT reaction by catalyzing nucleic acid structural rearrangements at various steps in the synthetic process (*9*−*13*). To fully appreciate the biological roles and functional significance of retroviral NC proteins, it is necessary to understand their nucleic acid binding and

†This research was partially supported by NIH Grant ES-02662 (A.H.M.).

* Author to whom correspondence should be addressed.

‡ University of California.

§ National Cancer Institute−Frederick Cancer Research and Development Center.

|| Recipient of a fellowship from the Subdirección General de Promoción de la Investigación, Ministerio de Educación y Ciencia (Spain).

⊗ Abstract published in *Advance ACS Abstracts,* October 1, 1997.

[1] Abbreviations: Aro, aromatic amino acid; CT, charge transfer; EA, electron affinity energy; EcoSSB, single-stranded DNA binding protein from *E. coli*; EG, ethylene glycol; HIV-1, human immunodeficiency virus, type 1; IN, integrase; IP, ionization energy; k_i, decay rate constant of the T_i sublevel; MIDP, microwave-induced delayed phosphorescence; MoMuLV, Moloney murine leukemia virus; NC, nucleocapsid; ODMR, optically detected magnetic resonance; p7, nucleocapsid protein of HIV-1; RT, reverse transcriptase; SIV, simian immunodeficiency virus; SLR, spin−lattice relaxation; t_0, delay time between the end of optical pumping and the start of data accumulation in the delay ODMR measurement; W_{ij}, spin−lattice relaxation rate constant for the transition, $T_i \rightarrow T_j$; zfs, zero field splittings.

S0006-2960(97)00676-4 CCC: $14.00

structural properties at various stages of the replication cycle.

In general, mature NC proteins are small (50−70 residues), highly basic (p*I* greater than 9) proteins that bind to single-stranded nucleic acids (*14*). NC proteins of all known retroviruses (except members of the Spumavirus class) have 1 or 2 copies of a conserved amino acid sequence consisting of 10 variable residues (X) and 4 invariant residues, Cys $(X)_2$ Cys $(X)_4$ His $(X)_4$ Cys. The invariant residues function to coordinate a zinc ion through histidine imidazole and cysteine thiolates, forming CCHC-type zinc fingers (*15, 16*) which provide the Gag precursors and the mature NC proteins with highly organized structures that facilitate nucleic acid binding. The variable residues (X) distinguish the CCHC-type zinc fingers associated with specific NC proteins but nevertheless exhibit conserved features such as the placement of aromatic residues (Trp, Tyr, Phe, and His). NC proteins with one CCHC-type zinc finger have two aromatic residues (Aro) in the sequence, i.e., Cys Aro X Cys $(X)_4$ His Aro $(X)_3$ Cys where the first Aro residue is Tyr or Phe and the second is Trp. The Moloney murine leukemia virus (MoMuLV) NC protein is the prototype for the single-fingered NC proteins. Lentiviruses have two CCHC zinc fingers per NC protein, each containing one aromatic residue in the sequence, i.e., Cys X Aro Cys $(X)_4$ His $(X)_4$ Cys. HIV-1 and simian immunodeficiency virus (SIV) NC proteins are the prototypes for this class. HIV-1 NC protein contains Phe in the first zinc finger and Trp in the second, whereas SIV NC protein has Trp in both zinc fingers.

Fluorescence spectroscopy has been applied in a number of instances to the study of the structural and nucleic acid-interactive properties of the NC protein from HIV-1 (*10, 17−20*) and of other retroviruses (*7, 21, 22*).

The phosphorescent triplet state properties of the indole ring have been used in the characterization of a large number of proteins (*23−25*). Single-stranded nucleic acid-binding proteins often utilize aromatic side chains in hydrophobic (stacking) interactions with exposed nucleic acid bases. In previous studies, we have made use of the luminescence properties of tryptophan and the technique of optically detected magnetic resonance (ODMR) to show that Trp residues in the NC proteins of MoMuLV (*26*) and HIV-1 (*27, 28*) stack with nucleotide bases when the proteins interact with single-stranded nucleic acids. Since it probes the properties of the excited triplet state in detail, ODMR is a technique particularly well-suited to assess the occurrence of aromatic stacking between Trp side chains and nucleobases. Among the aromatic amino acids, tryptophan has been shown to result in the largest stabilization energy as a result of base stacking (*29*).

Figure 1 shows the principal axis system and triplet sublevel energy level diagram of tryptophan indicating the zero field splittings (zfs) and decay pattern that normally is observed. We have reported previously on phosphorescence and ODMR measurements of p7 and on its complexes with several polynucleotide substrates (*27, 28*). Complex formation with polynucleotides produces a red-shift in the phosphorescence of Trp37, located in the C-terminal zinc finger domain of p7, and a reduction in the phosphorescence lifetime that is manifested mainly in a larger k_x, the decay constant of the T_x sublevel. The intersystem crossing pattern also is altered toward increasing the relative populating rate of the T_x sublevel. The phosphorescence red-shift is found to increase monotonically with an increase in the binding

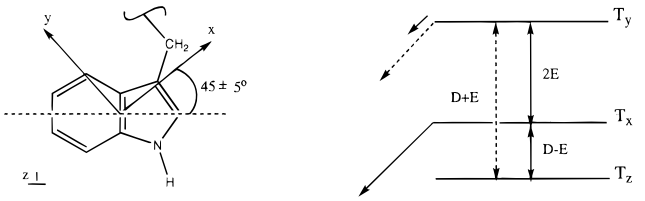

FIGURE 1: Structure of the tryptophanyl side chain showing the orientation of the principal magnetic axes of the phosphorescent triplet state. Also shown is its zero field energy level diagram. Solid and dashed single-headed arrows represent phosphorescence and intersystem crossing, respectively. Solid double-headed arrows are the readily observable ODMR transitions, while the dashed double-headed arrow indicates the normally weak or unobservable ODMR transition.

affinity of p7 with the substrate. A red-shift in the phosphorescence of tryptophan in rigid media is associated with increased local polarizability and reduced polar interactions (*30*) which would be expected to occur, for instance, in moving an aqueous solvent-exposed tryptophan to the interior of a globular protein or if the residue became subject to aromatic stacking interactions. In our previous work (*27, 28*), the spectral shifts of Trp37 in p7 when bound to polynucleotides were attributed to stacking interactions with the nucleobases. The correlation of their magnitude with binding affinity to the homopolymers that was observed suggested that stacking interactions of Trp37 contribute significantly to the stability of polynucleotide complexes of p7.

A previously studied example of such an interaction occurs in poly(dT) complexes of the single-stranded DNA binding protein from *E. coli*, EcoSSB. We have made measurements on a series of mutant EcoSSB's in which one or more of the tryptophans is replaced by phenylalanine, a residue less effective in aromatic stacking. We find that Trp54 specifically undergoes a large, *ca*. 4 nm phosphorescence red-shift when EcoSSB binds to poly(dT) and that the W54F mutant binds with the smallest affinity of any of the four single point mutations (W → F) at Trp positions (*31, 32*). Subsequent ODMR measurements (*33, 34*) reveal that binding to poly(dT) leads to a 4-fold increase in the k_x of Trp54 as well as a selective enhancement of intersystem crossing to T_x. The triplet sublevel kinetics of Trp54 are perturbed to such an extent that polarity reversals of the steady-state ODMR signals result. Furthermore, the zfs of Trp54, in particular the *D* parameter, are reduced significantly as a result of electronic delocalization in the triplet state. These observations suggest that aromatic stacking interactions of Trp54 contribute to the stabilization of EcoSSB complexes with poly(dT), and that these interactions are manifested, as outlined above, in the triplet state properties of this residue.

In the earlier work on p7−nucleic acid complexes (*27, 28*), acquisition of high-quality ODMR signals was hampered by the effect of binding to the polynucleotide substrates on the intensity of the steady-state ODMR signals of Trp37. These signals were reduced in most samples to barely detectable levels. This behavior was attributed to the unfortunate effect of complex formation on the sublevel populating and decay kinetics that reduces drastically the steady-state sublevel population differences. Since ODMR depends on the existence of these population differences (*24, 25, 35*), the signals become difficult to observe. ODMR signals were observed previously (*28*) *during the decay of*

phosphorescence, however, since the sublevels decay at different rates producing transient population differences. But the transition frequencies obtained from these delayed ODMR measurements were not very reliable since we did not have an algorithm at that time to relate the observed transient response to the parameters of interest, i.e., the band center frequency, ν_0, and the bandwidth, $\nu_{1/2}$. Recently we have developed a theoretical expression that does just this, allowing us to use a personal computer to fit the shape of the delayed ODMR response to the parameters ν_0 and $\nu_{1/2}$ (*36*).

In this paper, we report the results of new delayed ODMR measurements on an extended series of nucleic acid complexes of p7 in which this algorithm is used to obtain reliable ODMR frequencies and bandwidths. Also, we have employed a newly developed method of global analysis of microwave-induced delayed phosphorescence (MIDP) data (*37*) to obtain sublevel decay rate constants and relative intersystem crossing rates that are not influenced by spin−lattice relaxation (SLR). These kinetic data along with the SLR rate constants are reported for p7 complexes in this paper.

These new analytical methods (*36*, *37*) have been applied recently to studies of nucleic acid binding by the NC protein of MoMuLV (*26*).

MATERIALS AND METHODS

Materials. The p7 NC protein from HIV-1/MN (p7) was obtained as described earlier (*28*). Briefly, HPLC fractions containing p7 (identified by PAGE mobility, Western blotting, and N-terminal sequencing) were collected, pooled, and lyophilized. p7 was resuspended in the presence of excess Zn(II), and its concentration was calculated based on optical absorbance and amino acid analysis measurements. This solution was aliquoted into sterile polypropylene vials and relyophilized. Concentrations were determined spectrophotometrically using $\epsilon^{280} = 5.7 \times 10^3$ cm^{-1} M^{-1}.

The oligonucleotides d(TG)$_2$, d(TG)$_4$, d(IT)$_2$, d(IT)$_4$, d(UG)$_4$, and d(G)$_8$ were synthesized by the Recombinant DNA Laboratory at SAIC Frederick using phosphorimidite precursors. The oligonucleotides d(I)$_4$, d(I)$_8$, and d(I)$_{16}$ were synthesized from phosphorimidite precursors by the Protein Structure Laboratory at UC Davis. r(G)$_8$ was purchased from Macromolecular Resources (Fort Collins, CO). Poly(A), poly(C), poly(U), poly(I), and poly(dT) were purchased as lyophilized samples from commercial sources. All polynucleotides were obtained from Pharmacia, except for poly(A) which was from Sigma. Polynucleotide and oligonucleotide concentrations were obtained spectrophotometrically using the following extinction coefficients: ϵ^{259}(A) = 15.4 $\times 10^3$; ϵ^{271}(C) = 9.1 $\times 10^3$; ϵ^{260}(U) = 7.4 $\times 10^3$; ϵ^{249}(I) = 12.7 $\times 10^3$; ϵ^{260}(T) = 12.7 $\times 10^3$; ϵ^{253}(G) = 13.7 $\times 10^3$ in units of cm^{-1} M^{-1}.

Methods. Equilibrium binding isotherms for the association of p7 with nucleic acid lattices were obtained by monitoring changes in the fluorescence emission intensity of its sole Trp residue upon complex formation. Measurements were carried out in either a Shimadzu 5000U or a Spex FluoroMax-2 spectrofluorometer, with excitation at 288 nm (3 nm bandwidth) and emission at 355 nm (10 nm bandwidth). Titrations were performed at 25 °C in 10 mM sodium phosphate, pH 7.0, by stepwise addition of oligonucleotide aliquots to a p7 solution. p7 was kept at a concentration of 0.8 or 3 μM in a dual path length (0.2 $\times$ 1.0 cm) Suprasil quartz cuvette (Uvonic Instruments). The fractional protein saturation was inferred from a salt-back titration carried out by progressive addition of 5 M NaCl solution to the p7−nucleic acid complex. Binding constants were derived at each ionic strength and represented as a double-logarithmic plot of log K *vs* log [Na$^+$] (*38*−*40*).

Equilibrium binding constants were calculated either from Scatchard plots derived from fluorescence quenching measurements carried out upon nucleic acid additions at 10 mM sodium phosphate ("reverse titrations") or from "salt-back titrations" in which a nucleocapsid protein−oligonucleotide complex (preformed at low ionic strength, 1 mM sodium phosphate) was disrupted by addition of aliquots of concentrated NaCl (*38*−*40*). In the instances that the reverse titrations could be directly analyzed (binding was neither stoichiometric nor too weak), they gave results in agreement with the salt-back titration method (which was generally applicable). The binding affinity of nucleocapsid protein for weakly-interacting nucleic acids lattices could only be measured from double-logarithmic representations of binding affinity *vs* monovalent ion concentration. Since the p7 association constant increases by 200-fold (on average) by decreasing the ionic strength 10-fold (e.g., 1 mM *vs* 10 mM sodium phosphate), limiting fluorescence quenching at saturation in 1 mM sodium phosphate could be directly determined or easily extrapolated in all cases. Light absorption by the nucleic acid was minimized by presenting the cuvette's short path length (0.2 cm) to the excitation beam. Inner filter effects (usually resulting in about 5% absorption of incident light) were corrected in the determination of binding affinity. Binding determinations were carried out at least in triplicate, with an average standard deviation of *ca.* 40% of the values quoted below in this paper.

Phosphorescence measurements were made at 77 K using excitation by a 100 W high-pressure Hg arc lamp whose output was filtered through a monochromator set at 295 nm using 16 nm band-pass. Red-edge excitation (excitation monochromator set at 313 nm with further filtering by a WG 320-2 cutoff filter) was used when required to help discriminate between tryptophan sites. The phosphorescence/ODMR spectrometer, now using photon counting, has been described recently (*37*, *41*). ODMR experiments were carried out in the absence of an applied magnetic field at the temperature of pumped liquid He, 1.2 K in our apparatus, in order to minimize SLR.

The lyophilized samples were dissolved in 10 mM phosphate buffer, pH 7.2. Complexes were formed by adding an aliquot of p7 solution to the nucleic acid solution and mixing for 10 min; 30% v/v ethylene glycol (EG) was added as cryosolvent prior to making spectroscopic measurements, except for d(G)$_8$ and r(G)$_8$ when 50% v/v EG was added. Attempts to prepare samples containing p7 complexes of poly(G) were unsuccessful due to precipitation of the polynucleotide upon initial addition of protein. For r(G)$_8$, all glassware and plastic ware were treated with the RNase inhibitor diethyl pyrocarbonate, 0.1% in water, for at least 12 h at 37 °C, rinsed with sterile water, and then autoclaved for 15 min at 15 lb/in.^{2} on the liquid cycle. Buffer and doubly distilled water were passed through a 0.22 μm sterile filter before use. Concentrations of p7 in the samples ranged

between 0.2 and 0.4 mM while the ratio of nucleic acid phosphate to p7 was between 10:1 and 25:1.

The delayed slow-passage ODMR experiment and its analysis to obtain ν_0 and $\nu_{1/2}$, the band center frequency and its half-width at half-height, respectively, have been described earlier (*36*). Signal accumulation is started after a delay, t_0, following cessation of optical pumping. After an additional delay of 2−3 s, in order to accumulate base line data, the microwave sweep is begun. Fitting of the delayed ODMR response also yields "apparent sublevel decay constants", which incorporate the effects of SLR. Recent work suggests (*36, 37*) that the apparent decay constants obtained in the analysis of delayed slow-passage ODMR responses approximate the eigenvalues of the rate constant matrix. In cases where all three ODMR band centers ($D - E$, $2E$, and $D + E$) of tryptophan could be obtained, the zero field splitting parameters, D and E, were obtained from the expressions:

$$D = [\nu_0(D + E) + \nu_0(D - E)]/2 \quad (1)$$

$$E = [\nu_0(D + E) + \nu_0(2E) - \nu_0(D - E)]/4 \quad (2)$$

In order to obtain the actual sublevel decay constants, k_x, k_y, and k_z, we employed global analysis of MIDP data sets (*37*) which typically involves the least-squares fitting of ca. 20 000 data points. The MIDP data sets for more than one magnetic resonance transition cannot be fitted globally without the inclusion of SLR in the analytical expression. Thus, if two or all three of the transitions are analyzed globally, both the decay rate constants and the SLR rate constants can be determined. Global analysis of MIDP data was used whenever possible in this work to obtain the sublevel decay constants as well as the SLR rate constants. For those samples where both the decay constants and SLR rate constants could be obtained, the global MIDP analysis also was used to obtain the relative sublevel populating rate constants. These quantities, reflecting the effect of complex formation on the intersystem crossing pathways of Trp37, also are reported for these samples.

EXPERIMENTAL RESULTS

Fluorimetric Equilibrium Binding Isotherms. The intrinsic Trp fluorescence emission of HIV-1 p7 was significantly quenched upon association with nucleic acid lattices. For homopolymeric octanucleotides, the limiting fluorescence quenching at saturation ranged from 42% for A to 98% for I (Table 1). All the alternating-base octanucleotides screened as eventual ligands in ODMR studies [$d(GA)_4$, $d(IT)_4$, $d(TG)_4$ and $d(UG)_4$] quenched the p7 fluorescence by 95−99% (Table 1). The binding stoichiometry was consistent with a 1:1 complex for all octanucleotides. Tetranucleotides bound with a 2 oligo:1 NC p7 stoichiometry and lower affinity, and induced a limiting quenching of smaller extent than the corresponding octanucleotides (Table 1). log $K°$ is obtained from the abscissa intercept of the rectilinear trace in a double-logarithmic plot (not shown) of log K_{obs} *vs* log [Na^+], and does not reflect the contribution of electrostatic interactions between the nucleic acid and p7 since it is calculated at 1 M NaCl (the thermodynamic reference state). The ionic dependence of the binding affinity can be estimated from the slope, $\delta \log K_{obs}/\delta \log [Na^+]$, of such double-logarithmic representations (Table 1). For the alternating-base tetranucleotides, the slope is 1.93 ± 0.04, whereas for the octanucleotides it averages 2.28 ± 0.23 (the density of counterions bound in the thermodynamic sense to the polyelectrolyte backbone of the oligo depends on the base−base distance, which does not vary significantly with sequence). The average ionic dependence for the homopolymeric octanucleotides is 2.22 ± 0.56, similar to that of the heterogeneous sequence oligos. With an average counterion density of 0.7 monovalent cation per phosphate in single-stranded lattices, the ionic dependence parameter suggests a displacement of 3 sodium ions per bound p7 molecule (in the absence of anion uptake or release).

Table 1: Binding of HIV-1 p7 to Homopolymeric and Alternating-Base DNA Oligonucleotides

system[a]	ΔF_{lim}	slope[b]	log $K°$ (1 M Na^+)	K_{obs} (13 mM Na^+)
$d(A)_8$	0.42	−1.27	1.69	1.2×10^4
$d(U)_7T$	0.92	−2.13	1.60	4.1×10^5
$d(T)_8$	0.85	−2.34	1.71	1.3×10^6
$d(I)_8$	0.98	−2.38	3.05	3.5×10^7
$d(G)_8$	0.75	−3.00	2.71	2.3×10^8
$d(GA)_4$	0.95	−2.47	2.75	2.5×10^7
$d(IT)_2$	0.93	−1.97	2.28	9.8×10^5
$d(IT)_4$	0.98	−2.50	3.35	1.2×10^8
$d(TG)_2$	0.97	−1.89	3.12	4.9×10^6
$d(TG)_4$	0.97	−1.94	4.29	8.9×10^7
$d(UG)_4$	1.00	−2.21	4.08	1.7×10^8

[a] Binding stoichiometry is 1:1 for octanucleotides, 2 oligo:1 p7 for tetranucleotides. [b] $\delta(\log K_{obs})/\delta$ (log [Na^+]).

All alternating-base oligonucleotides bind with micromolar to low nanomolar K_{obs} in 10 mM sodium phosphate, pH 7.0 (Table 1), whereas the homopolymeric sequences exhibit a broader range in binding constants. Under the conditions used in ODMR studies, p7 should be quantitatively (>99%) bound to all homo- and heteropolymeric sequences except perhaps $d(A)_8$, where fractional saturation between 79 and 99% was achieved.

Phosphorescence Results. The phosphorescence spectra of p7 and its complexes with each of the polyribonucleotides, and with $r(G)_8$, are shown in Figure 2. The 0,0-band of Trp37 is a prominent feature in each spectrum. A phosphorescence component originating from adenine, the 0,0-band at 387 nm, also is present in the spectrum of the poly(A) complex, while a weak blue-shifted background assigned to cytosine is seen in the poly(C) complex. A red-shift of the 0,0-band peak of Trp37 is apparent in the spectra of these complexes, the largest shift, ca. 6.6 nm, occurring in the complex with poly(I). The Trp37 0,0-band peak wavelengths of p7 and each of these complexes are given in Table 2. Phosphorescence red-shifts of Trp37 in complexes with poly(dT) and the oligodeoxynucleotides were found also (spectra not shown). The greatest red-shifts, as large as 10 nm, are found in $d(IT)_4$ and $d(IT)_2$ complexes (see below). These data also are listed in Table 2.

Delayed Slow-Passage ODMR Results. Examples of delayed slow-passage spectra of the Trp37 $D - E$ transition of p7 and its complexes with poly(U) and poly(I) are shown in Figure 3. The superimposed solid lines are least-squares fittings yielding the ν_0 and $\nu_{1/2}$ values given in Table 2. The apparent decay constants and relative radiative rate constants that are also produced by the analysis (*36*) are presented in Table 3 only for the samples whose MIDP data sets could not be successfully analyzed globally. Examples of delayed slow-passage spectra of the $2E$ and $D + E$ transitions of the

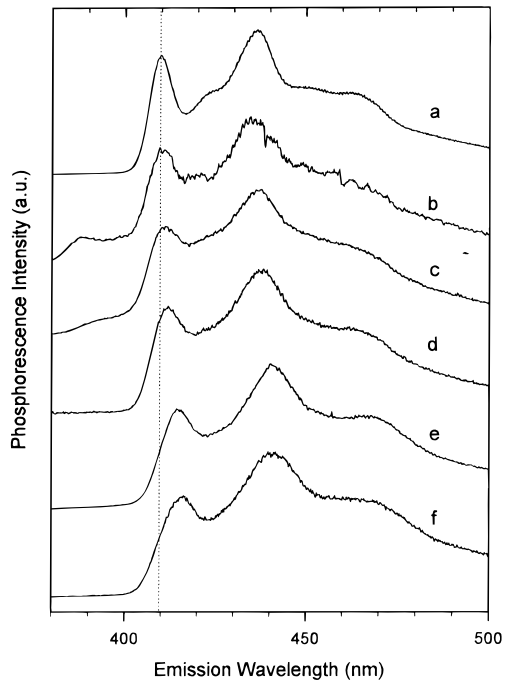

FIGURE 2: Phosphorescence spectra of (a) p7, (b) p7 + poly(A), (c) p7 + poly(C), (d) p7 + poly(U), (e) p7 + $r(G)_8$, and (f) p7 + poly(I) in EG−buffer glass at 77 K. Samples are excited at 295 nm with 16 nm bandwidth and observed at 3.2 nm resolution.

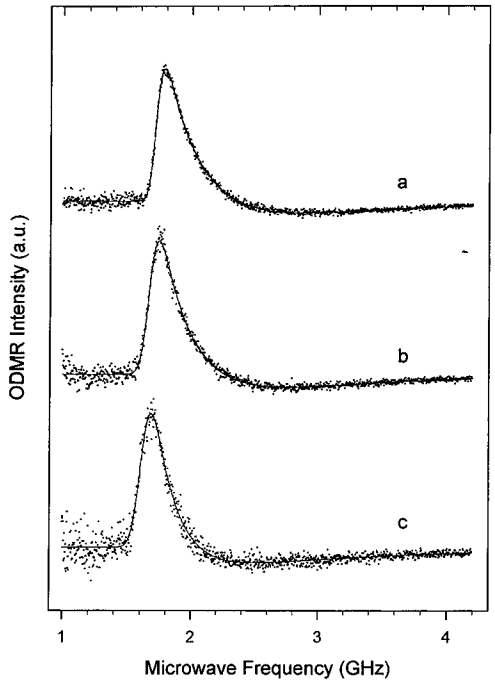

FIGURE 3: Delayed slow-passage ODMR spectra of the $D - E$ transition of Trp37 in (a) p7, (b) p7 + poly(U), and (c) p7 + poly(I) in EG−buffer glass measured at 1.2 K. The microwave sweep started at 1.3 GHz; its rate was 100 MHz/s with t_0 = (a) 4, (b) 3, and (c) 2 s. The microwave frequency was limited to the $D - E$ region by a 2 GHz low-pass filter. The superimposed solid lines represent the best fit of each response based on parameters given in Table 1.

poly(U) and poly(I) complexes are shown in Figures 4 and 5, respectively. The superimposed calculated responses are based on least-squares fittings (band center and half-width data listed in Table 2) and apparent rate constants and radiative properties of the appropriate sublevels (not given).

It should be pointed out that although only one example of a delayed slow passage spectrum is given for each sample in Figures 3 through 5, each experiment was repeated typically 4 or 5 times using different microwave sweep rates and sweep delay times. The values of ν_0 and $\nu_{1/2}$ given in Table 2 are mean values from separate analysis of each data set. The standard deviations are determined largely by the variance in these analyses.

The complex of p7 with poly(A) presents a special case in that ODMR signals from adenine were observed along with those of Trp37. Delayed ODMR measurements made monitoring the emission of poly(A) at 387 nm (Figure 2) allowed us to determine the response of the adenine triplet state. The response of poly(A) for a given sweep rate and delay was then subtracted from the data of the complex to yield the response of Trp37. It proved possible to resolve the Trp37 response from that of poly(A) in the $D - E$ and $2E$ signal regions, since these bands were sufficiently

Table 2: Triplet State Properties of Trp37 in HIV-1 p7 and Its Complexes with Nucleic Acids[a]

		$D - E$		$2E$		$D + E$				$(\Delta D \times 10^6)/$
sample	$\lambda_{0,0}$ (nm)[b]	ν_0 (GHz)	$\nu_{1/2}$ (MHz)	ν_0 (GHz)	$\nu_{1/2}$ (MHz)	ν_0 (GHz)	$\nu_{1/2}$ (MHz)	D (GHz)	E (GHz)	$\Delta E_{0,0}$
p7	409.6	1.721(3)	51.5(9)	2.489(1)	122(2)	4.222(5)	89(10)	2.972	1.247	−
p7 + poly(A)	410.0	1.709(6)	56(4)	2.503(5)	267(38)	*c*	*c*	2.961	1.251	*d*
p7 + poly(C)	411.0	1.689(4)	74(1)	2.533(7)	156(24)	4.225(12)	148(51)	2.957	1.267	6.0
p7 + poly(U)	411.8	1.675(2)	65(2)	2.515(3)	127(13)	4.176(7)	124(9)	2.925	1.254	12.0
p7 + poly(dT)	412.0	1.676(2)	59(1)	2.493(4)	132(13)	4.162(5)	139(4)	2.919	1.245	12.4
p7 + rG_8	415.0	1.680(1)	68.5(9)	2.520(6)	116(4)	4.226(8)	148(33)	2.953	1.266	2.0
p7 + poly(I)	416.2	1.616(3)	70(2)	2.622(2)	179(8)	4.139(14)	170(31)	2.878	1.286	8.1
p7 + $d(UG)_4$	413.6	1.675(1)	54(1)	2.499(3)	121(4)	4.184(11)	79(30)	2.930	1.252	5.9
p7 + $d(TG)_2$	414.2	1.684(2)	58(3)	2.484(2)	118(61)	4.178(6)	109(8)	2.931	1.245	5.0
p7 + dG_8	414.4	1.683(2)	65(3)	2.514(4)	109(5)	4.219(36)	79(29)	2.951	1.263	2.5
p7 + $d(TG)_4$	414.6	1.679(5)	63(2)	2.468(8)	101(3)	4.152(5)	112(15)	2.916	1.235	6.3
p7 + $d(IT)_4$	417.8[e]	1.546(4)	45(4)	2.787(2)	92(7)	[4.122(11)][g]	[91(22)]	2.834	1.341	7.8
	415.8[f]	1.647(9)	66(8)	2.567(6)	161(8)			2.884	1.261	8.0
p7 + $d(IT)_2$	418.4[e]	1.564(8)	54(4)	2.690(36)	95(13)	[4.115(25)][g]	[98(31)]	2.840	1.310	7.1
	416.6[f]	1.668(9)	49(9)	2.473(28)	117(20)			2.891	1.230	6.5
p7 + dI_{16}	415.4	1.632(4)	74(2)	2.552(7)	157(3)	4.153(3)	122(7)	2.891	1.268	7.9
p7 + dI_8	416.2	1.604(5)	91(6)	2.617(6)	161(6)	4.184(36)	164(14)	2.894	1.299	6.7
p7 + dI_4	417.0	1.582(1)	84(6)	2.684(25)	181(16)	4.149(4)	180(49)	2.865	1.313	8.2

[a] The standard deviation (σ) in last digit given in parentheses. [b] Tryptophan 0,0-band peak, measured at 77 K, λ_{exc} = 295 nm except as otherwise indicated. [c] Superimposed with adenine's bands. [d] Not evaluated due to large uncertainty in ΔD. [e] Measured at 1.2 K. [f] Red-edge excitation at 1.2 K, see text. [g] Measured using 295 nm excitation. Used in calculation of D and E for both sites.

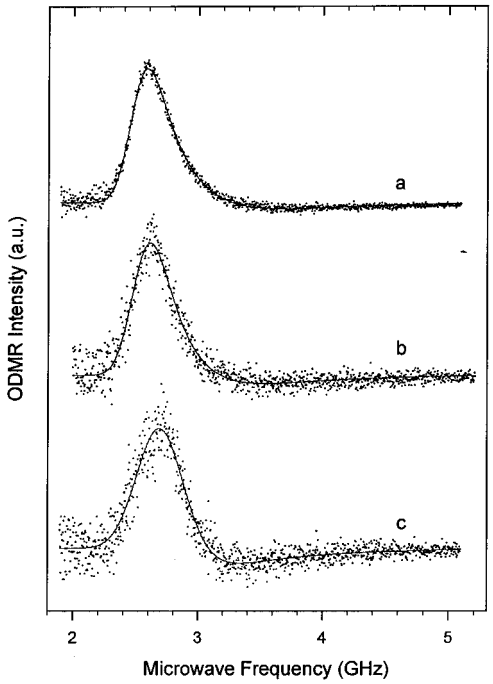

FIGURE 4: Delayed slow-passage ODMR spectra of the 2*E* transition of Trp37 in (a) p7, (b) p7 + poly(U), and (c) p7 + poly(I) in EG−buffer measured at 1.2 K. The microwave sweep started at 2.2 GHz; its rate was 100 MHz/s with t_0 = (a) 1, (b) 0.15, and (c) 0.15 s. The microwave frequency was limited to the 2*E* signal region by a 3.0 GHz low-pass filter. The superimposed solid lines represent the best fit of each response based on parameters given in Table 2.

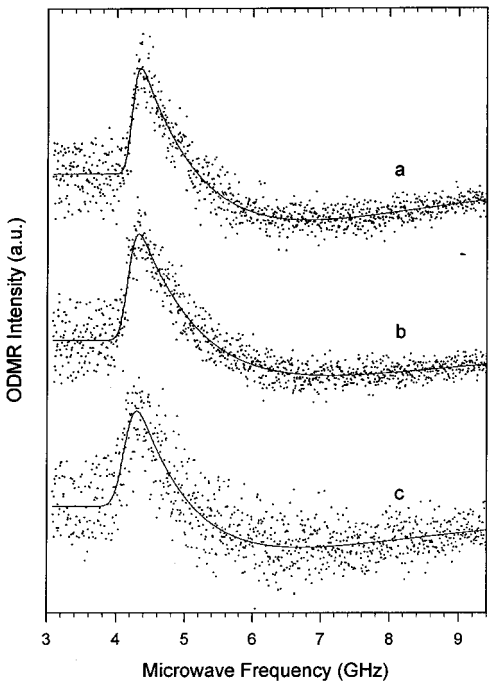

FIGURE 5: Delayed slow-passage ODMR spectra of the $D + E$ transition of Trp37 in (a) p7, (b) p7 + poly(U), and (c) p7 + poly(I) in EG−buffer glass measured at 1.2 K. The microwave sweep started at 3.6 GHz; its rate was 200 MHz/s with t_0 = (a) 15, (b) 13, and (c) 11 s. The microwave output is limited by a 5.0 GHz low-pass filter. The superimposed solid lines represent the best fit of each response based on parameters given in Table 2.

separated and of comparable intensity, but not so for the $D + E$ signal region where the ODMR intensity is dominated by adenine.

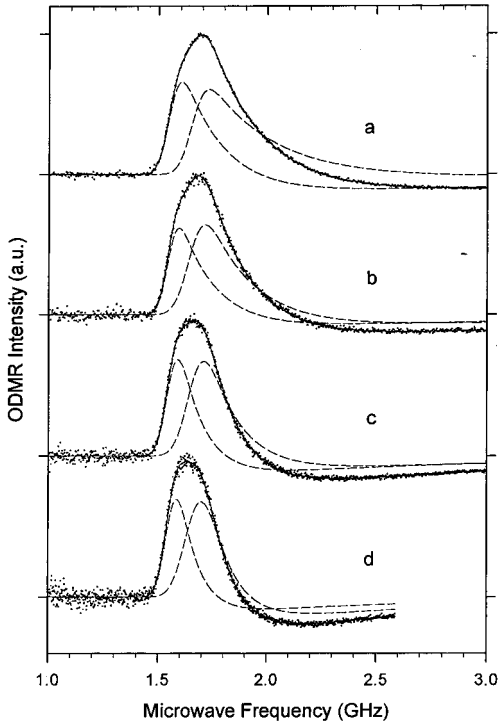

FIGURE 6: Delayed slow-passage ODMR spectra of the $D - E$ transition of Trp37 in the p7 complex of $d(IT)_4$. Excitation was at 295 nm using 16 nm bandwidth; the emission was monitored at 417.8 nm with 3.2 nm bandwidth. The microwave frequency, started at 1.2 GHz, was swept at (a) 133, (b) 100, (c) 80, and (d) 50 MHz/s with t_0 = 2 s. The dashed lines represent the individual responses of Trp37 at two sites calculated from parameters given in Table 2. The solid line superimposed on the data is the sum of the two best-fit responses.

Results of the analysis of similar delayed slow-passage ODMR experiments on p7 complexes with the oligodeoxynucleotides are given in the lower half of Table 2. Particularly interesting results were obtained with the p7 complexes of $d(IT)_2$ and $d(IT)_4$. In both of these complexes, the $D - E$ and 2*E* signals of Trp37 were found to occur as partially resolved doublets. Spectra of the $D - E$ signals and 2*E* signals of the $d(IT)_4$ complex, each measured at four different microwave sweep rates, are shown in Figures 6 and 7, respectively. The best-fit responses based on data listed in Table 2 are superimposed on the data as solid lines. The contributions of the individual sites to the overall signal are shown by the dashed curves. In order to assign the signals to specific sites, an excitation wavelength-selection measurement was carried out. The resulting steady-state slow-passage ODMR spectra are shown in Figure 8. Red-edge excitation in the singlet absorption band leads to a *blue-shift* in the phosphorescence 0,0-band peak (Table 2), and a reduction in the relative intensity of the lowest frequency (negative polarity) $D - E$ band as well as of the highest frequency 2*E* band. Thus, the site with the lowest value of $D - E$ and the highest value of E is associated with a red-shifted phosphorescence origin. A similar result is obtained for the p7 complex of $d(IT)_2$ (spectra not shown).

Microwave-Induced Delayed Phosphorescence; Triplet State Kinetics. A set of MIDP data for the $D - E$ and 2*E* microwave transitions of Trp37 in the p7 complex of poly(dT) is shown in Figure 9. The sublevel decay constants and SLR rate constants obtained from global analysis (*37*) of the approximately 11 000 data points are listed in Table 3. The rate constants obtained for the other samples whose

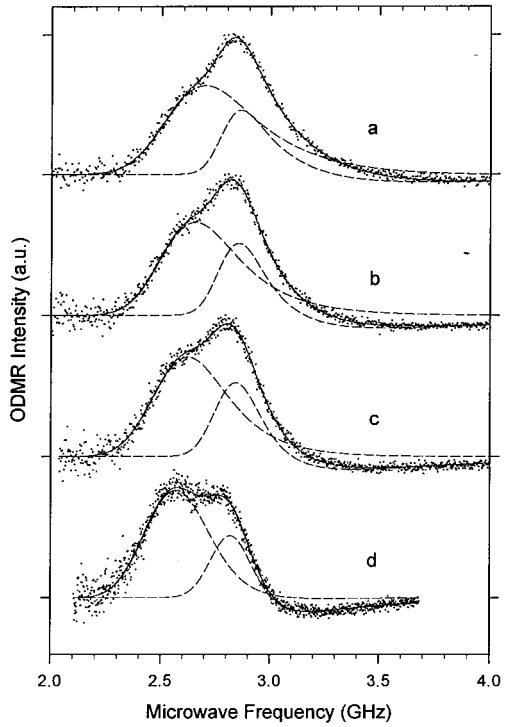

FIGURE 7: Delayed slow-passage ODMR spectra of the 2*E* transition of Trp37 in the p7 complex with $d(IT)_4$. Conditions of excitation and emission are the same as in the Figure 6 caption. The microwave frequency, started at 2.2 GHz, was swept at (a) 133, (b) 100, (c) 80, and (d) 50 MHz/s with $t_0 = 0.15$ s. The dashed lines represent the calculated individual responses of Trp37 at two sites using parameters given in Table 2. The solid line superimposed on the data is the sum of the two best-fit responses.

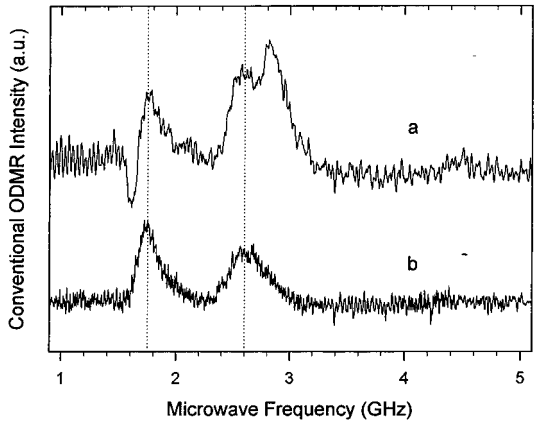

FIGURE 8: Conventional ODMR spectra of Trp37 in the p7 complex with $d(IT)_4$. (a) Excitation and emission conditions as in the caption of Figure 6. (b) Red-edge excitation using a 313 nm excitation monochromator setting with 16 nm bandwidth along with a WG 320-2 cutoff filter. Emission was monitored at 0,0-band maximum (415.8 nm) with 3.2 nm band-pass. The microwave sweep rate was 112.5 MHz/s. Vertical dashed lines indicate the observed peaks of spectrum b.

MIDP were subjected successfully to global analysis are listed, as well. Global analysis was not possible for p7 complexes of poly(A) and poly(C) because of interference from nucleic acid phosphorescence, or for complexes of $d(IT)_2$ and $d(IT)_4$ because the two sites (see above) could not be resolved in a MIDP experiment. For these samples, the decay constants listed are the "apparent decay constants" from analysis of the delayed ODMR responses; they are influenced by SLR.

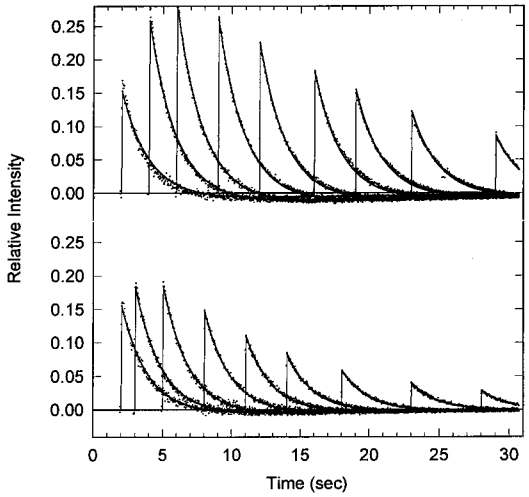

FIGURE 9: MIDP responses of Trp37 in the p7 complex with poly(dT) at various delay times for the $D - E$ transition (upper set) and the 2*E* transition (lower set). The phosphorescence was monitored at the 0,0-band peak (Table 1). Superimposed on the data points are the MIDP responses calculated by global analysis using the best-fit kinetic parameters listed in Table 3.

The k_i and W_{ij}, $i,j = x, y, z$, taken together form the elements of the rate constant matrix, **R**, from which one can obtain the sublevel populating vector, **P**, by solving

$$\mathbf{P} - \mathbf{R}\cdot\mathbf{n^0} = \mathbf{0} \tag{3}$$

where $\mathbf{n^0}$ is the vector of steady-state populations and **0** is the null vector (*37*). If the duration of optical pumping is sufficiently long, then the initial populations at the beginning of the MIDP measurement may be used as the elements of $\mathbf{n^0}$; best-fit values for the initial populations result from the global least-squares analysis. Thus, **P** can be obtained by solving eq 3. Since normally only the relative values of the $\mathbf{n^0}$ elements are obtained, only the relative values of the elements of **P** can be obtained. We have listed the calculated relative values, P_i, for the samples analyzed by MIDP in Table 4.

DISCUSSION

Binding Affinity Studies. The binding affinity of p7 for short oligonucleotides of various sequence was characterized thermodynamically. Among these, certain alternating-base sequences exhibit a surprisingly tight binding that was unexpected on the basis of the affinity of p7 for homopolymeric lattices of the same length. The sequence discrimination of HIV-1 p7 is based on hydrophobic interactions that contribute to the binding free energy of the association to a larger extent than the electrostatic interactions. The former include stacking of aromatic side chains with nucleic acid bases and (in the case of alternating-base sequences) possibly hydrogen bonding.

The lower affinity for p7 of tetranucleotides, relative to larger oligonucleotides, can be attributed to two underlying causes: (i) incomplete fulfillment of the protein's nucleic acid binding site in the shorter sequences [the interactive binding site size of p7 has been proposed to span a minimum of five nucleotide bases (*42*)]; and (ii) a lower net release of counterions from the nucleic acid polyphosphate backbone due to the larger contribution of end effects in the shorter lattices. Mechanism (i) decreases the standard binding free

Table 3: Kinetic Parameters of Trp37 in HIV-1 p7 and Its Complexes with Nucleic Acids

sample	τ (s)[a]		k_x (s^{-1})[b]	k_y (s^{-1})[b]	k_z (s^{-1})[b]	W_{xy} (s^{-1})[b]	W_{xz} (s^{-1})[b]	W_{yz} (s^{-1})[b]
p7	6.4(100)		0.35(3)	0.09(1)	0.000(8)	0.04(1)	0.06(2)	0.05(3)
p7 + poly(A)[c]	6.1(30)	2.0(64)	0.33(4)	0.15(1)	0.04(2)	–	–	–
p7 + poly(C)[c]	5.8(70)	0.14(17)	0.48(1)	0.26(1)	0.05(8)	–	–	–
p7 + poly(U)	5.8(77)	2.5(15)	0.46(4)	0.16(2)	0.00(1)	0.00(1)	0.04(2)	0.054(2)
p7 + poly(dT)	5.3(65)	2.5(26)	0.48(2)	0.126(8)	0.008(6)	0.005(6)	0.028(8)	0.040(1)
p7 + rG_8	4.7(66)	1.5(24)	0.60(5)	0.17(3)	0.00(2)	0.00(2)	0.03(2)	0.061(4)
p7 + poly(I)	4.8(56)	2.2(34)	0.66(6)	0.14(3)	0.00(2)	0.02(3)	0.00(3)	0.045(4)
p7 + $d(UG)_4$	5.5(57)	2.0(28)	0.65(4)	0.13(2)	0.04(2)	0.00(2)	0.01(2)	0.034(3)
p7 + $d(TG)_2$	5.2(29)	4.9(69)	0.45(4)	0.10(1)	0.006(8)	0.04(1)	0.05(2)	0.051(2)
p7 + dG_8	4.5(63)	1.9(27)	0.76(17)	0.13(8)	0.00(6)	0.02(8)	0.05(8)	0.051(9)
p7 + $d(TG)_4$	5.6(60)	4.2(35)	0.54(2)	0.16(1)	0.000(8)	0.000(7)	0.03(1)	0.048(1)
p7 + $d(IT)_4$[c]	4.9(73)	2.6(21)	0.67(8)[d]	0.11(4)[d]	0.053(5)[d]	–	–	–
			0.46(2)[e]	0.32(6)[e]	0.051(5)[e]			
p7 + $d(IT)_2$[c]	3.4(55)	1.4(38)	0.75(24)[d]	0.19(4)[d]	0.056(3)[d]	–	–	–
			0.43(14)[e]	0.20(4)[e]	0.09(2)[e]			
p7 + dI_{16}	5.1(75)	2.7(20)	0.50(2)	0.123(9)	0.000(8)	0.014(8)	0.05(1)	0.041(2)
p7 + dI_8	4.7(62)	2.4(32)	0.65(11)	0.10(4)	0.05(6)	0.02(5)	0.03(7)	0.010(1)
p7 + dI_4	4.6(64)	2.1(28)	0.67(4)	0.13(2)	0.03(2)	0.00(2)	0.02(2)	0.025(2)

[a] Phosphorescence decays was measured at 77 K. The two major components are listed with the preexponential factor, in percent, in parentheses. [b] The standard error (σ) in last digit given in parentheses. Measurements made at 1.2 K. From global analysis of MIDP data except as noted. [c] Apparent values of decay constants from delayed ODMR analysis. Not corrected for SLR. [d] Species with red-shifted emission having small $D - E$ and large $2E$ values, cf. Table 2. [e] Species with blue-shifted emission having large $D - E$ and small $2E$ values, cf. Table 2.

Table 4: Relative Sublevel Populating Rates for Trp37 in HIV-1 p7 and Its Complexes with Nucleic Acids [a]

sample	P_x	P_y	P_z
p7	0.50(7)	0.50(8)	0.00(3)
p7 + poly(U)	0.67(6)	0.33(4)	0.00(2)
p7 + poly(dT)	0.72(2)	0.27(2)	0.01(1)
p7 + rG_8	0.73(6)	0.22(4)	0.05(3)
p7 + poly(I)	0.77(8)	0.23(4)	0.00(2)
p7 + $d(UG)_4$	0.81(5)	0.15(3)	0.04(2)
p7 + $d(TG)_2$	0.77(8)	0.21(3)	0.02(2)
p7 + dG_8	0.80(9)	0.14(5)	0.06(6)
p7 + $d(TG)_4$	0.74(3)	0.25(2)	0.01(2)
p7 + dI_{16}	0.67(3)	0.33(4)	0.00(2)
p7 + dI_8	0.84(12)	0.08(4)	0.07(8)
p7 + dI_4	0.87(4)	0.10(2)	0.03(2)

[a] The standard error (σ) in last digit given in parentheses.

energy ($\Delta G° = -RT \ln K°$) for the shorter oligos, due to the smaller contribution of hydrophobic interactions in the binding process (log $K°$ column in Table 1).

Among the alternating-base DNA oligonucleotides, UG and TG are by far the best ligands for p7. Notably, we treat $d(TG)_4$ as a specific sequence for p7, since it exhibits a binding affinity that exceeds the weighted average for $(dT)_8$ and $(dG)_8$ [(*42*) and manuscript in preparation]. In fact, the binding affinity in the standard state ($K°$) for $d(TG)_4$ is about 150 times that expected based on its base composition (log $K_{av}° = [\log K°(dT_8) + \log K°(dG_8)]/2$). This supernumerary $K°$ affinity is reduced 10-fold in $d(IG)_4$ which differs only in the loss of an exocyclic amine group (perhaps involved in a hydrogen bonding with p7) in I, relative to G. $d(GA)_4$, on the other hand, exhibits the expected $K°$ calculated from the average of $(dG)_8$ and $(dA)_8$, and we do not assume $d(GA)_4$ to be a specific sequence for p7. Note that the binding preference exhibited by p7 toward alternating (TG) oligos is determined primarily by an increase in the hydrophobic component. This is the dominant contribution to the binding free energy, which ranks as A ~ C (not shown in Table 1) < U ~ T < G ~ I for homopolymeric octadeoxyribonucleotides.

Phosphorescence and ODMR. The complexes of p7 with both homo- and heteropolymeric oligonucleotides were investigated by phosphorescence and ODMR spectroscopy. It is clear from the results reported above that all of the measurable parameters of the Trp37 triplet state are altered by binding p7 to the polynucleotide and oligonucleotide substrates.

Specifically, the phosphorescence spectrum undergoes a red-shift, the magnitude of which varies with the substrate (Table 2). Both the *D* and the *E* parameters are altered by binding. We find, in each case, that a decrease in *D* accompanies substrate binding, whereas changes in *E*, both increases and decreases, generally are smaller. Large increases of *E* are found, however, for some of the oligonucleotide complexes, particularly the most red-shifted complexes of p7 with $d(IT)_2$ and $d(IT)_4$ (Table 2).

Comparison of Triplet State Kinetics and the Phosphorescence Red-Shift. In addition to the spectral shifts discussed above, substrate binding leads also to changes in the triplet sublevel kinetics of Trp37. As can be seen in Table 3, the overall phosphorescence decay kinetics measured at 77 K become more rapid as a result of complex formation and they are markedly nonexponential, in contrast with free p7. The 1.2 K global MIDP results (Table 3) are in accord with the 77 K decay measurements and also show that it is largely k_x that is enhanced by nucleic acid binding. [The apparent enhancements of k_y in the poly(A), poly(C), $d(IT)_2$, and $d(IT)_4$ complexes are not real, since these values are from delayed ODMR analysis, and thus are affected by SLR]. It should be noted that $k_z = 0$ within experimental error for each sample measured by MIDP, confirming earlier results (*37*) that the T_z sublevel of tryptophan is depopulated largely by SLR rather than by direct decay to the ground state. The intersystem crossing patterns revealed in Table 4 suggest that this sublevel also may be populated to a great extent by SLR.

The phosphorescence red-shift as well as the decrease in phosphorescence lifetime is the result of increased local polarizability that may result from aromatic stacking interactions. We have plotted the red-shift in cm^{-1} *vs* k_x for all samples whose MIDP could be measured and analyzed. When we examined the data from the individual MIDP measurements on the guanine-containing oligonucleotides,

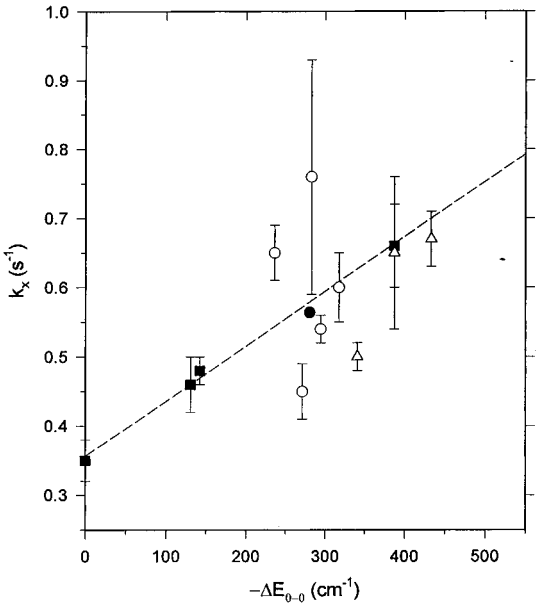

FIGURE 10: Plot of k_x *vs* the phosphorescence 0,0-band red-shift for p7 and each of its nucleic acid complexes subjected to global MIDP analysis. Data for p7 and polynucleotide complexes are indicated by solid squares, complexes with the guanine-containing oligonucleotides are open circles, and the weighted centroid of these oligonucleotide data (see text) is indicated by the filled circle. The oligo(I) complexes are indicated by triangles. Also plotted is the least-squares regression line obtained from p7 and the polynucleotide data; $k_x = 0.3566 - 7.936 \times 10^{-4}\ \Delta E_{0,0}\ s^{-1}$. $r^2 = 0.9966$.

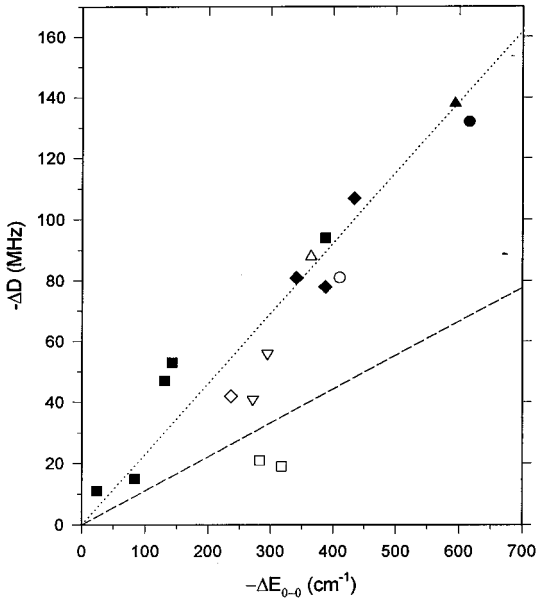

FIGURE 11: Plot of the zfs shift ($-\Delta D$) *vs* the phosphorescence red-shift ($-\Delta E_{0,0}$) for p7 complexes of the nucleic acids. (■) Polynucleotide complexes; (◆) $d(I)_n$, $n = 4, 8, 16$; (□) $d(G)_8$, $r(G)_8$; (▽) $d(TG)_4$ and $d(TG)_2$; (◇) $d(UG)_4$; (△) and (▲) resolved sites of $d(IT)_4$; (○) and (●) resolved sites of $d(IT)_2$. The dashed line represents $\Delta D/\Delta E_{0,0} = 3.7 \times 10^{-6}$, the slope exhibited by tryptophan in aqueous ethylene glycol glass. The dotted line represents $\Delta D/\Delta E_{0,0} = 7.7 \times 10^{-6}$, its average for poly(I), dI_4, dI_8, and dI_{16}.

we found a great deal of scatter. Examination of these data (Tables 2 and 3) reveals that the phosphorescence red-shifts fall within a rather narrow range while the k_x vary greatly. This behavior could result from a diversity of specific interactions that characterize the complexes of p7 with these oligonucleotides and may be lost or averaged out in polynucleotide complexes. With this in mind, we also have plotted the data of the guanine-containing oligonucleotides as a single point at the centroid of the five individual points, weighting the k_x values by the reciprocal of σ (Table 3). These data, plotted in Figure 10 along with p7, the polynucleotide, and the oligo(I) data, show that k_x correlates extremely well with the phosphorescence red-shift, $-\Delta E_{0,0}$, for the complexes. The centroid of the guanine data falls close to the regression calculated from p7 and the polynucleotide data. Except for dI_{16}, the oligo(I) complexes correlate well with the other data.

Comparison of Zero Field Splitting Shifts and Phosphorescence Red-Shifts. Increased polarizability of the environment leads not only to a phosphorescence red-shift but also to a decrease in the zfs. This indicates that the triplet state electron distribution becomes more diffuse in an increasingly polarizable environment resulting in a decrease of the magnetic dipole−dipole interaction that controls the size of the zfs. Furthermore, the environment- or solvent-induced red-shift and zfs shift are theoretically predicted, as well as found experimentally, to be linearly correlated with a positive dimensionless slope ($\Delta D/\Delta E_{0,0}$) of the order 10^{-6}−10^{-5} (*43*−*45*). This theoretical model uses solvent−molecule interactions to perturb the phosphorescent state, resulting in an admixture of more highly excited triplet states that are *localized on the molecule*. Both a lowering of the unperturbed energy of the phosphorescent state and a reduction of the zfs result, since the higher energy admixed triplet states generally are expected to be more diffuse than the phosphorescent state. The shifts are predicted to be linearly related.

The zfs D parameter, which is positive for $^3(\pi,\pi^*)$ states of extended aromatic systems, usually is taken as an indication of changes in electron delocalization. Normally, $D \gg |E|$, the latter being a measure of the in-plane anisotropy of the triplet state wave function. In terms of the interelectron distance, r, and its Cartesian components (coordinates in Figure 1 for tryptophan), the zfs parameters are given by

$$D = (3/4)(\gamma h/2\pi)^2\langle(r^2 - 3z^2)/r^5\rangle_{av} \quad (4)$$

$$E = (3/4)(\gamma h/2\pi)^2\langle(y^2 - x^2)/r^5\rangle_{av} \quad (5)$$

where γ is the electron magnetogyric ratio and h is Planck's constant. If the wave function expands uniformly, then both D and E will decrease proportionately. For tryptophan, however, solvent-induced red-shifts (in the absence of aromatic stacking interactions) lead to a decrease in D, and an *increase* in E. For tryptophan, the measured slopes (*46*) are $\Delta D/\Delta E_{0,0} = 3.7 \times 10^{-6}$, and $\Delta E/\Delta E_{0,0} = -3.6 \times 10^{-6}$. The large value of E in tryptophan is attributed to considerable localization of the triplet electron pair in the ethylenic region of the five-membered ring, contributing significantly to the in-plane anisotropy (eq 5). The increase in E with solvent red-shift is consistent with an enhancement of spin density in the ethylenic bond and may be associated with solvent-induced mixing of localized excited triplet states with a high degree of ethylenic character. This effect on E may overcome the overall reduction of the zfs which is reflected in the decreasing value of D with solvent red-shift. Thus, we will use the zfs D parameter to characterize the admixed excited states.

We have plotted ΔD *vs* $\Delta E_{0,0}$ for each of the p7−nucleic acid complexes in Figure 11. In the case of the p7 complexes

of the oligonucleotides $d(IT)_2$ and $d(IT)_4$, we have plotted the data for the redder and bluer sites separately. Although the $\lambda_{0,0}$ of the bluer emission (that arose from red-edge excitation) can be associated with a unique site since only a single tryptophan ODMR spectrum is found (Figure 8), the same is not true of the redder emission produced by excitation at 295 nm because this gives rise to ODMR signals from both sites with comparable intensity (Figures 6, 7, and 8). In order to compensate for this, we assumed that the peak wavelength *of the redder site* actually lies to the red of the combined emission peak wavelength by an amount that is equal to the difference between the latter and the bluer peak (arising from red-edge excitation). Thus, the peak wavelengths of the *most red-shifted sites* of $d(IT)_2$ and $d(IT)_4$ were assumed to be located at 420.2 and 419.8 nm, respectively. The dashed line in Figure 11 represents a slope of 3.7×10^{-6} which is exhibited by tryptophan in 50% (v/v) ethylene glycol−water glass (*46*) where the solvent shifts do not involve aromatic stacking interactions. It is clear that most of the data points lie above this line, and thus have values of $\Delta D/\Delta E_{0,0}$ in excess of 3.7×10^{-6}. In the last column of Table 2, we list the value of $\Delta D/\Delta E_{0,0}$ for each sample.

We propose that in these p7−nucleic acid complexes, values of $\Delta D/\Delta E_{0,0}$ in excess of that exhibited by tryptophan in nonaromatic solvent (3.7×10^{-6}) result because charge transfer (CT) character is admixed into the phosphorescent state as a consequence of aromatic stacking interactions. Admixture of charge transfer states into the phosphorescent state will reduce the zfs to a far greater extent than a comparable admixture of triplet states localized on the molecule. CT states in a typical nonaromatic solvent are too high in energy to mix significantly into the triplet state, but in stacked tryptophan−nucleic acid complexes, such states may be low enough energetically to admix and to reduce significantly the zfs. A relevant example of the effectiveness of CT effects in reducing the zfs is provided by the isomeric naphthalenophanes, a number of whose triplet state zfs and phosphorescence red-shifts have been measured (*47*, *48*). In these compounds, a pair of naphthalene units are maintained rigidly in a face-to-face arrangement by covalent bridging groups. The transannular interactions between π-electrons lead to luminescence red-shifts and reductions in D. The red-shift increases with the extent of $\pi-\pi$ overlap. Calculations point to significant triplet state CT character in the naphthalenophanes (*49*) as well as in paracyclophanes (*50*), although the phosphorescent state remains mostly localized on one or the other unit. For a set of 12 naphthalenophanes of varying geometries (*48*), $\Delta D/\Delta E_{0,0} = 15\ (\pm 6) \times 10^{-6}$. On the other hand, from solvent shifts induced in naphthalene by 3-methylpentane glass, Gradl et al. (*44*) find $\Delta D/\Delta E_{0,0} = 5 \times 10^{-6}$, a slope not very different from that exhibited by tryptophan in aqueous EG, and only about one-third the value exhibited by the naphthalenophanes. This example suggests that the value of $\Delta D/\Delta E_{0,0}$ may be diagnostic of the extent of CT character mixed into the triplet state by aromatic stacking interactions.

For a tryptophan residue interacting with nucleic acids, the extent of CT character in the triplet state will increase with the degree of overlap of the π-electron distribution of the unperturbed triplet state with the π-electrons of the nucleobase, and decrease with increasing energy of the nearest charge transfer triplet state (*49*, *50*). Assuming that the lowest energy CT triplet state arises from electron transfer from tryptophan to a nucleobase $^3(Trp^+N^-)$, its energy will be determined by

$$E_{CT} = IP(Trp) - EA(N) + C \qquad (6)$$

where IP and EA are ionization and electron affinity energies, and C consists of Coulomb and polarization energy. CT in the opposite direction is energetically less favorable because $IP(N) \gg IP(Trp)$ for each N (*51*, *52*). More positive values of EA(N) will lead to enhanced CT character in the tryptophan triplet state, given comparable $\pi-\pi$ overlap, and thus to larger values of $\Delta D/\Delta E_{0,0}$.

An experimental value of EA(N) is available only for uracil for which the gas phase vertical electron affinity was found to be −0.19 eV (*53*). However, electron affinity energies of the nucleobases (excluding hypoxanthine, the chromophore of inosine) have been calculated recently using *ab initio* molecular orbital methods (*54*) to give vertical EA's of −1.23, −0.74, −0.40, −0.32, and −0.19 eV, for G, A, C, T, and U, respectively. The adiabatic EA's of G and A are predicted to be negative as well, suggesting that the anions of G and A are unstable with respect to ionization in the vapor. The vertical IP of skatole (3-Me-indole) has been found experimentally to be 7.54 eV (*51*). This value can be used for IP(Trp) in eq 6. If we estimate $C \approx -3$ eV for a localized CT state, $^3(Trp^+N^-)$, we find that E_{CT} will vary between a maximum of 5.8 eV for G and a minimum of 4.7 eV for U. With respect to the localized tryptophan triplet state (3.0 eV), the CT states of G and U π-complexes can be estimated to have ΔE_{CT} of *ca*. 2.8 eV and 1.7 eV, respectively. These estimates of ΔE_{CT} (particularly for U) are small enough to suggest that significant CT character may be admixed with the tryptophan triplet state by transannular π-electron interactions in a stacked complex. The energies of the CT states of other bases should lie between these limits with ΔE_{CT} increasing in the order $U < T < C < A \ll G$.

Homopolymer and Homooligomer Complexes. For stacked complexes of tryptophan with the homopolymers and homooligomers, we predict that to the extent that charge transfer character influences the triplet state zfs, the value of $\Delta D/\Delta E_{0,0}$ should increase in the order $G < A < C < T < U$. Comparing these quantities (Table 2), we find that $\Delta D/\Delta E_{0,0}$ increases in the order $G < C < I < T \approx U$. This quantity could not be evaluated with certainty for the poly(A) sample because both ΔD and $\Delta E_{0,0}$ are so small that their uncertainties dominate the ratio. The uncertainty in D is particularly large because the $D + E$ transition frequency could not be used in its evaluation. Because both shifts are so small, we think that if a stacked complex of p7 forms with poly(A), stacking must be minor, and the CT contribution to the triplet state is negligible. The lack of strong interactions between adenine and Trp37 is in accord with the small limiting fluorescence quenching of p7 by $d(A)_8$ that is observed (Table 1). Since the fluorescence measurements were carried out in the absence of cryosolvent, it is possible that the latter could inhibit binding in the low-temperature experiments. This possibility is most likely for poly(A). The values of $\Delta D/\Delta E_{0,0}$ for poly(I) and the oligoinosines all are very similar and large, falling between those of poly(C) and poly(U). The large red-shift suggests a significant degree of transannular π-electron interactions due to aromatic stacking. It is

interesting that $|\Delta E_{0,0}|$ increases in the order $d(I)_{16} < d(I)_8 < d(I)_4$, suggesting that the stacking between Trp37 in the complex with p7 increases in this order. This may stem from a lower energy of base destacking in the shorter oligos due to end effects. The energy of complex formation with p7 probably does not change very much with oligomer length once the binding site size has been reached (*ca*. five bases) whereas the base−base unstacking energy may still increase beyond this oligomer size. Although the EA of hypoxanthine has not been calculated or measured, our data suggest that it has a value between those of C and U. Finally, the data for $d(G)_8$ and $r(G)_8$ suggest that although stacking interactions are present, there is little if any CT character admixed into the triplet state by transannular π-electron interactions.

Heterooligomer Complexes. Complexes of p7 with $d(IT)_2$ and $d(IT)_4$ are of two distinguishable types. Complexes characterized by the larger $|\Delta E_{0,0}|$ present a more polarizable environment at the Trp37 binding site, probably as the result of enhanced transannular π-electron interactions. These complexes also have the largest $|\Delta D|$ of all the samples discussed here, which is also consistent with strong transannular π-electron interactions that admix CT character into the triplet state. The complexes with the smaller $|\Delta E_{0,0}|$ plot close to poly(I) on Figure 11. For both types, $\Delta D/\Delta E_{0,0}$ falls in the same range as that spanned by the poly(I) and inosine homooligomer complexes (Table 2, Figure 11), suggesting that the major stacking interactions in these heterooligomers occur with hypoxanthine bases.

The p7 complexes of $d(UG)_4$, $d(TG)_2$, and $d(TG)_4$ have values of $\Delta D/\Delta E_{0,0}$ intermediate between those exhibited by poly(dT), or poly(U), and dG_8. The phosphorescence red-shifts exceed those of the poly(dT) and poly(U) complexes, being more nearly comparable to those of the G oligomers. The ΔD values, on the other hand, resemble those found for the poly(dT) and poly(U) complexes. We think that stacking of Trp37 with G must occur in these heterooligomer complexes, although transannular interactions with T or U must be present as well, leading to CT character comparable to that found in the poly(dT) and poly(U) complexes.

Triplet State Populating Kinetics. Although the MIDP measurements give no information about the effect of nucleic acid complexing on the *absolute* sublevel populating rates, it can be seen from the data in Table 4 that the pattern of relative populating rates is affected significantly by complex formation. Both polynucleotide and oligonucleotide binding lead to an increase in P_x relative to P_y. A similar effect of binding poly(dT) to EcoSSB is seen for Trp54 (*33*), in which case P_x increases from ca. 0.5 to >0.9. It is worthy of note that $P_z \approx 0$ for all of the samples in this study. Previous estimates of P_z for tryptophan that have not been able to compensate for SLR, e.g., Zang et al. (*33*), have overestimated this quantity.

The intersystem crossing pathways as well as the radiative decay of the triplet state are controlled by internal spin−orbit coupling, specifically by its effect of mixing singlet state character into triplet sublevels (*55, 56*). Symmetry plays an important role in this pattern; it is noteworthy that it is k_x as well as P_x of Trp37 that are selectively enhanced by nucleic acid binding to p7. It also is significant that both k_z and $P_z \sim 0$. The latter observation is readily understood from the fact that the *z*-component of the spin−orbit coupling operator is vanishingly small in $^3(\pi,\pi^*)$ states (*57, 58*). The major portion of the intersystem crossing and phosphorescence is induced by the in-plane (*x* and *y*) components of the spin−orbit coupling operator (*57, 58*), which in the case of tryptophan mix the T_x and T_y sublevels with highly excited $^1(\sigma,\pi^*)$ and $^1(\pi,\sigma^*)$ states (see Figure 1). The stacking interactions involved in the binding of nucleic acids to p7 appear to enhance only the effects of the *x*-component of spin−orbit coupling, possibly by reducing selectively the energy of those excited singlet states that are coupled with T_x by this operator.

The possibility also exists that nucleic acid binding of p7 is accompanied by triplet−triplet energy transfer to Trp37. This could serve as a sublevel-specific populating mechanism that operates in parallel with intersystem crossing. We have found in other protein−nucleic acid complexes that the efficiency of triplet−triplet energy transfer is reduced severely when the temperature is lowered into the liquid He temperature range (M. C. Prieto and A. H. Maki, unpublished results). The contribution of energy transfer to the populating kinetics cannot be ruled out, however, in the present case.

CONCLUSIONS

Phosphorescence and ODMR measurements have been made on complexes of p7 with several polynucleotides and oligonucleotides using improved instrumentation and newly developed analytical algorithms. The chromophore studied in this work is Trp37, located in the C-terminal zinc finger region of the protein. The patterns of zfs changes of Trp37 with phosphorescence red-shift ($-\Delta E_{0,0}$) are consistent with the occurrence of aromatic stacking interactions in both polynucleotide and oligonucleotide complexes, as previously reported (*27, 28*). Furthermore, in this study the value of $\Delta D/\Delta E_{0,0}$ is used diagnostically to gauge the extent of CT character mixed into the triplet state by transannular π-electron interactions in stacked complexes. Values of $\Delta D/\Delta E_{0,0}$ in excess of 3.7×10^{-6} (the value exhibited by tryptophan in aqueous ethylene glycol glass) are the consequence of CT admixture, while the magnitude of $\Delta E_{0,0}$ itself increases with that of the transannular π-electron interactions. Values of $\Delta D/\Delta E_{0,0}$ measured for the homopolymers and homooligomers increase in the order $G \ll C < I < T \approx U$, the same order as the EA of these bases (other than hypoxanthine, for which EA data are not available). The Trp37 phosphorescence red-shift, on the other hand, increases in the order $A < C < U \approx T < G < I$. Based on our measurement of $\Delta D/\Delta E_{0,0}$, we predict that the EA of I lies between those of C and U. Stacking interactions of the Trp residue of p7 with poly(A) appear to be negligible.

Two types of complex with differing red-shift and zfs have been resolved when p7 binds to either $d(IT)_2$ or $d(IT)_4$. $\Delta D/\Delta E_{0,0}$ is effectively the same for both types and similar to that of poly(I), suggesting that the principal interactions of Trp37 occur with I in these heterooligomers. Inosine-containing oligos induce the largest phosphorescence spectral red-shift, and increase in k_x. Each of these effects is predicted to be of larger magnitude for a more intimate aromatic stacking interaction with nucleic acid bases. (The magnitude of ΔD depends also on the accessibility of nucleic acid CT states and thus on the EA of the base, but it should scale with the degree of stacking for a given base.) Indeed, $d(I)_8$ exhibits the largest value of $\log K^\circ$ (3.05 ± 0.16) among all deoxyoctanucleotides investigated, suggesting that aromatic stacking is strongest for this base ($\log K^\circ$ is related to the

binding free energy in the standard state, 1 M NaCl, and its value increases with the contribution of hydrophobic interactions to the binding process).

In the case of the G-containing heterooligomers, $d(UG)_4$, $d(TG)_2$, and $d(TG)_4$, the red-shifts resemble those observed for $r(G)_8$ and $d(G)_8$, while the ΔD is similar to that found in the poly(dT) and poly(U) complexes. This suggests transannular interactions of Trp37 with both G and T (or U), but with the CT admixture originating from T (or U) in these complexes.

Recent experimental results suggest that p7 can associate with nucleic acids in at least two different binding modes: alternating-base sequences, including $(IT)_n$ and $(TG)_n$, exhibit specific nucleic acid binding (*42*). $(TG)_n$ and $(GT)_n$ oligonucleotides bind p7 with comparable affinity but significantly more tightly than $(IT)_n$ oligos (*42*), suggesting the involvement of the exocyclic amino group of G in a favorable interaction (possibly a hydrogen bond) with nucleocapsid protein. It is tempting to speculate that the two spectral sites seen in p7−$d(IT)_n$ complexes may correspond to dissimilar Trp37 local microenvironments induced by the two binding modes. In one of these, a charged or hydroxyl-bearing group that may participate in hydrogen bonding with G could undergo a closer in-plane (edge-on) approach to the I ring due to its lack of exocyclic NH_2. This would result in a more polarizable environment that could induce a more pronounced phosphorescence red-shift as well as a larger perturbation of the *E* zfs parameter.

Complex formation is accompanied by a selective increase of k_x, which correlates linearly with $\Delta E_{0,0}$ in the homopolymer complexes. Also observed is an increase in P_x, the relative intersystem crossing rate to the T_x sublevel. Both effects are believed to arise from stacking interactions that enhance selectively the effectiveness of the *x*-component of the spin−orbit coupling. The mechanism may involve stabilization of localized singlet states that are coupled with T_x.

$|\Delta E_{0,0}|$ of p7 complexes increases in the order $dI_{16} < dI_8 < dI_4$, suggesting that stacking of Trp37 increases accordingly. Although k_x and P_x are similar for dI_4 and dI_8 complexes, both are considerably smaller for the dI_{16} complex. Stacking of Trp37 with nucleobases may be impeded in the latter case by competition with stronger interbase stacking.

In summary, application of newly developed methodological protocols and analytical algorithms yields high-quality ODMR data that can be analyzed globally and result in a complete description of the zero field energy splittings and decay kinetics of the sublevels of the Trp triplet state in HIV-1 p7, both in the free state and in its complexes with various nucleic acid sequences. The more detailed knowledge thus gained on the photophysics of the excited triplet state of Trp37 in HIV-1 p7 allows us to attribute the changes in its triplet state properties observed upon formation of NC−nucleic acid complexes to a combination of two main factors: the extent of aromatic stacking with nucleobases (which parallels the protein's binding affinity for a given lattice) and the extent of admixture of charge transfer character into the triplet state (which varies with the electron affinity of the base). Notably, spectroscopic evidence reported here for the occurrence of two different bound structures in the complexes of HIV-1 p7 with certain alternating-base oligonucleotides can now be integrated with emerging thermodynamic and kinetic findings demonstrating the capacity of HIV-1 nucleocapsid protein to exhibit specific recognition for these sequences.

REFERENCES

1. Coffin, J. M. (1992) in *The Retroviridae* (Levy, J. A., Ed.) Vol. 1, pp 19−50, Plenum Press, New York.
2. Luciw, P. A. (1992) in *The Retroviridae* (Levy, J. A., Ed.) Vol. 1, pp 159−298, Plenum Press, New York.
3. Darlix, J.-L., Lapadat-Tapolsky, M., de Rocquigny, H., and Roques, B. P. (1995) *J. Mol. Biol. 254*, 523−537.
4. Gorelick, R. J., Nigida, S. M., Jr., Bess, J. W., Jr., Arthur, L. O., Henderson, L. E., and Rein, A. (1990) *J. Virol. 64*, 3207−3211.
5. Gorelick, R. J., Nigida, S. M., Jr., Arthur, L. O., Henderson, L. E., and Rein, A. (1991) in *Advances in Molecular Biology and Targeted Treatments for AIDS* (Kumar, A., Ed.) pp 257−272, Plenum Press, New York.
6. Henderson, L. E., Bowers, M. A., Sowder, R. C., Serabyn, S. A., Johnson, D. J., Bess, J. W., Jr., Arthur, L. O., Bryant, D. K., and Fenselau, C. C. (1992) *J. Virol. 66*, 1856−1865.
7. Karpel, R. L., Henderson, L. E., and Oroszlan, S. (1987) *J. Biol. Chem. 262*, 4961−4967.
8. Gorelick, R. J., Chabot, D. J., Ott, D. E., Gagliardi, T. D., and Arthur, L. O. (1996) *J. Virol. 70*, 2593−2597.
9. Wu, W., Henderson, L. E., Copeland, T. D., Gorelick, R. J., Bosche, W. J., Rein, A., and Levin, J. G. (1996) *J. Virol. 70*, 7132−7142.
10. Dib-Haij, F., Khan, R., and Giedroc, D. P. (1993) *Protein Sci. 2*, 231−243.
11. Ji, X., Klarmann, G. J., and Preston, B. D. (1996) *Biochemistry 35*, 132−143.
12. Pellska, J. A., Balasubramanian, S., Giedroc, D. P., and Benkovic, S. J. (1994) *Biochemistry 33*, 13817−13823.
13. You, J. C., and McHenry, C. S. (1994) *J. Biol. Chem. 269*, 31491−31495.
14. Long, C. W., Henderson, L. E., and Oroszlan, S. (1980) *Virology 104*, 491−496.
15. Berg, J. (1986) *Science 232*, 485−487.
16. Bess, J. W., Jr., Powell, P. J., Issaq, H. J., Schumack, L., Grimes, M. K., Henderson, L. E., and Arthur, L. O. (1992) *J. Virol. 66*, 840−847.
17. Summers, M. F., Henderson, L. E., Chance, M. R., Bess, J. W., Jr., South, T. L., Blake, P. R., Sagi, I., Perez-Alvarado, G., Sowder, R. C., III, Hare, D. R., and Arthur, L. O. (1992) *Protein Sci. 1*, 563−574.
18. Delahunty, M. D., South, T. L., Summers, M. F., and Karpel, R. L. (1992) *Biochemistry 31*, 6461−6469.
19. Mély, Y., Jullian, N., Morellet, N., De Rocquigny, H., Dong, C. Z., Piémont, E., Roques, B. P., and Gérard, D. (1994) *Biochemistry 33*, 12085−12091.
20. Mély, Y., De Racquigny, H., Morellet, N., Roques, B. P., and Gérard, D. (1996) *Biochemistry 35*, 5175−5182.
21. Mély, Y., Cornille, F., Fournié-Zaluski, M. C., Darlix, J. L., Roques, B. P., and Gérard, D. (1991) *Biopolymers 31*, 899−906.
22. Gelfand, C. A., Wang, Q., Randall, S., and Jentoft, J. E. (1993) *J. Biol. Chem. 262*, 18450−18456.
23. Kwiram, A. L. (1982) in *Triplet State ODMR Spectroscopy* (Clarke, R. H., Ed.) pp 427−478, Wiley-Interscience, New York.
24. Maki, A. H. (1984) in *Biological Magnetic Resonance* (Berliner, L., and Reuben, J., Eds.) Vol. 6, pp 187−293, Plenum Press, New York.
25. Maki, A. H. (1995) *Methods Enzymol. 246*, 610−638.
26. Wu, J. Q., Maki, A. H., Ozarowski, A., Urbaneja, M. A., Henderson, L. E., and Casas-Finet, J. R. (1997) *Biochemistry 36*, 6115−6123.
27. Lam, W.-C., Maki, A. H., Casas-Finet, J. R., Erickson, J. W., Sowder, R. C., II, and Henderson, L. E. (1993) *FEBS Lett. 328*, 45−48.
28. Lam, W.-C., Maki, A. H., Casas-Finet, J. R., Erickson, J. W., Kane, B. P., Sowder, R. C., II, and Henderson, L. E. (1994) *Biochemistry 33*, 10693−10700.

29. Kumar, N. V., and Govil, G. (1984) *Biopolymers 23*, 2009−2024.
30. Purkey, R. M., and Galley, W. C. (1970) *Biochemistry 9*, 3569−3574.
31. Khamis, M. I., Casas-Finet, J. R., Maki, A. H., Murphy, J. B., and Chase, J. W. (1987) *J. Biol. Chem. 262*, 10938−10945.
32. Casas-Finet, J. R., Khamis, M. I., Maki, A. H., and Chase, J. W. (1987) *FEBS Lett. 220*, 347−352.
33. Zang, L.-H., Maki, A. H., Murphy, J. B., and Chase, J. W. (1987) *Biophys. J. 52*, 867−872.
34. Tsao, D. H. H., Casas-Finet, J. R., Maki, A. H., and Chase, J. W. (1989) *Biophys. J. 55*, 927−936.
35. Clarke, R. H., Ed. (1982) *Triplet State ODMR Spectroscopy*, Wiley-Interscience, New York.
36. Wu, J. Q., Ozarowski, A., Davis, S. K., and Maki, A. H. (1996) *J. Phys. Chem. 100*, 11496−11503.
37. Ozarowski, A., Wu, J. Q., and Maki, A. H. (1996) *J. Magn. Reson. Ser. A 121*, 178−186.
38. Record, M. T., Jr., Lohman, T. M., and de Haseth, P. (1976) *J. Mol. Biol. 107*, 145−158.
39. Record, M. T., Jr., de Haseth, P., and Lohman, T. M. (1977) *Biochemistry 16*, 1791−1796.
40. de Haseth, P., Lohman, T. M., and Record, M. T., Jr. (1977) *Biochemistry 16*, 4783−4790.
41. Wu, J. Q., Ozarowski, A., and Maki, A. H. (1996) *J. Magn. Reson. Ser. A 119*, 82−89.
42. Urbaneja, M. A., Casas-Finet, J. R., Fisher, R. J., Rein, A., Bladen, S., Fivash, M., Gorelick, R. J., Kane, B. P., Arthur, L. O., and Henderson, L. E. (1997) *Biophys. J. 72*, A98.
43. van Egmond, J., Kohler, B. E., and Chan, I. Y. (1975) *Chem. Phys. Lett. 34*, 423−426.
44. Gradl, G., Friedrich, J., and Kohler, B. E. (1986) *J. Chem. Phys. 84*, 2079−2083.
45. Williamson, R. L., and Kwiram, A. L. (1988) *J. Chem. Phys. 88*, 6092−6106.
46. Von Schütz, J. U., Zuclich, J., and Maki, A. H. (1974) *J. Am. Chem. Soc. 96*, 714−718.
47. Schweitzer, D., Colpa, J. P., Behnke, J., Hausser, K. H., Haenel, M., and Staab, H. A. (1975) *Chem. Phys. 11*, 373−384.
48. Haenel, M. W., and Schweitzer, D. (1988) *Adv. Chem. Ser. 217*, 333−355.
49. Colpa, J. P., Hausser, K. H., and Schweitzer, D. (1978) *Chem. Phys. 29*, 187−199.
50. Hillier, I. H., Glass, L., and Rice, S. A. (1966) *J. Chem. Phys. 45*, 3015−3021.
51. Lias, S. G., Bartmess, J. E., Liebman, J. F., Holmes, J. L., Levin, R. D., and Mallard, W. G. (1988) *J. Phys. Chem. Ref. Data 17, Suppl. 1*.
52. Hush, N. S., and Cheung, A. S. (1975) *Chem. Phys. Lett. 34*, 11−13.
53. Compton, R. N., Yoshioka, Y., and Jordan, K. D. (1980) *Theor. Chim. Acta 54*, 259−260.
54. Sevilla, M. D., Besler, B., and Colson, A.-O. (1995) *J. Phys. Chem. 99*, 1060−1063.
55. Van der Waals, J. H., and de Groot, M. S. (1967) in *The Triplet State* (Zahlan, A. B., Ed.) pp 101−132, Cambridge University Press, Cambridge.
56. McGlynn, S. P., Azumi, T., and Kinoshita, M. (1969) *Molecular Spectroscopy of the Triplet State*, Prentice-Hall, Englewood Cliffs, NJ.
57. McClure, D. S. (1952) *J. Chem. Phys. 20*, 682−686.
58. Mizushima, M., and Koide, S. (1952) *J. Chem. Phys. 20*, 765−769.

BI970676F